Abdo *et al.*
Journal of Engineering and Applied Science (2024) 71:89
https://doi.org/10.1186/s44147-024-00424-8

Journal of Engineering and Applied Science

RESEARCH Open Access

Numerical assessment of using FRP rebars as an alternative passive reinforcement in RC beams

Marwan Abdo[1], Basem Abdelwahed[1*] and Salah El-Metwally[1]

*Correspondence:
bs_hadi@mans.edu.eg

[1] Mansoura University, Mansoura, Egypt

Abstract

Recent sustainable building strategies make the right decisions to be environmentally friendly and reduce carbon emissions. In some reinforced concrete (RC) elements, fiber-reinforced polymer (FRP) bars have been proposed as an alternative to conventional steel bars. The demand for using noncorrosive and/or nonmetallic reinforcing bars in various reinforced concrete projects has increased. Although these concrete elements are lightweight, have a long lifespan, and need little maintenance, their nonductile nature and bond with the surrounding concrete create significant challenges. Several experimental investigations have been conducted to evaluate the behavior of RC elements, even with their high cost. This study aims to assess numerically the viability of using FRP bars instead of traditional steel ones in simply supported reinforced concrete beams (RCBs) as longitudinal reinforcement (passive reinforcement). Utilizing the three-dimensional (3D) nonlinear finite element analysis (FEA) software (ABAQUS), a total of eighteen models were carried out to validate the results available in reference case studies with FRP bars. The verification of the numerical results has been verified by comparing them with the reference experimental data. Next, in order to assess the rigidity of such RCBs with FRP bars, parametric research was carried out. The numerical results proved that RCBs with FRP bars have a positive impact on enhancing load-carrying capacities. But on the other hand, the strain energy of such RCBs with CFRP bars is reduced to about 75% of the strain energy of RCBs with steel bars, which leads to low beam ductility.

Keywords: Reinforced concrete, Numerical modeling, Fiber-reinforced polymer (FRP), Carbon FRP rebar, Strain energy, Ductility

Introduction

With high durability, lightweight, and better fire resistance compared to RC structures with traditional bars, RC elements with composite materials made of polymers (FRP) are frequently used, as shown in Fig. 1a [1]. Among different RC elements, RC beams are the most commonly constructed elements as they require less reinforcing cage work with fewer bends. Because the extremities of such a beam do not have end hooks, the bond strength is a controlling parameter. If insufficient bond strength is

a: Various Applications of FRP Reinforcement [1]

b: Failure in RC beam with insufficient anchorage [2]

Fig. 1 Concrete structures with different reinforcing bars. **a** Various applications of FRP reinforcement [1]. **b** Failure in RC beam with insufficient anchorage [2]

given, brittle catastrophic failure resulting from slippage may occur, as shown in different damaged parts in Fig. 1b [2].

Traditionally, in the construction of RC structures, steel bars are used to resist tensile stresses. In the last decades, composite materials made of polymers (FRP) such as carbon, glass, basalt, or aramid fibers coated by resin matrix have been proposed as alternatives to conventional steel bars in concrete structures. Figure 2 clarifies the purpose of using FRP in structural engineering applications. FRP can be used in two ways: (1) for rehabilitation (i.e., for strengthening, repair, and retrofitting of existing structures) and (2) for a new composite FRP/concrete systems or a new construction with all FRP solutions [3]. In addition to being a non-corrosive material, FRP composites are nonmagnetic, lightweight, and have high strength [4]. Nevertheless, there may be some issues related to using FRP as a reinforcement, such as the ductility of structures, besides lack of yielding and the bars' low elastic modulus.

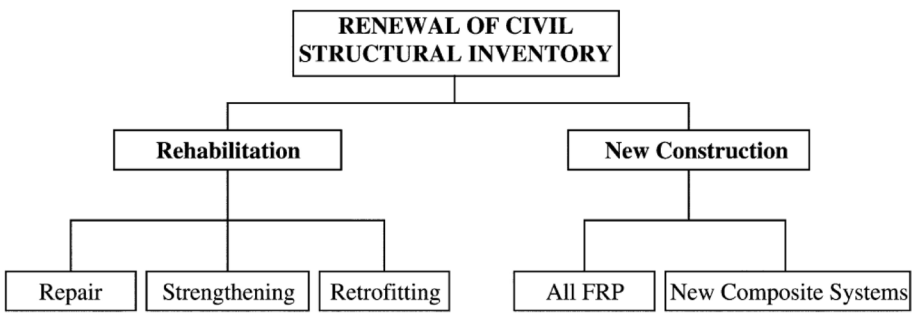

Fig. 2 The use of FRP in civil engineering [3]

Afifi (2013) [5] carried out a test of eleven loaded column specimens to investigate the behavior of RC columns with glass fiber-reinforced polymer (GFRP) compared to the traditional steel reinforcement. It was shown that RC columns with GFRP and steel bars behaved similarly, with a linear load–displacement behavior in the ascending part up to 85% of their failure loads. The average failure loads of the GFRP RC columns were 7% less than those of their steel RC counterparts. Abed (2021) [6] carried out a test of seven axially loaded column specimens to investigate their axial compression capacity and compare them with the experimental findings by Afifi (2013) [5]. It was shown that the numerical models of RC columns with GFRP bars and spirals produce good results in terms of the results of the experiments.

Adam et al. (2015) [7] investigated the effect of using bars from glass fiber-reinforced polymers (GFRP) in reinforcing concrete beams. It was shown that although the crack width tends to drop by 80% when increasing concrete strength from 25 to 70 MPa, it tends to decrease by 52% when increasing concrete strength from 25 to 45 MPa. Karayannis et al. [8] investigated the effect of using bars from carbon fiber-reinforced polymers (CFRP) in reinforcing concrete beams. It was demonstrated that the mid-span load–deflection curves have high pre-cracking flexural stiffness and decreased stiffness after cracking when compared to similar RCBs with steel bars. Additionally, it came to light that a shear failure instead of a pure flexural failure can occur when the CFRP reinforcement ratio is increased.

A numerical simulation of the experiments conducted by Adam et al. [7] and Karayannis et al. [8] was performed by Salih and Fangyuan [9]. The conclusions of the nonlinear finite element modeling and the experimental data agreed, according to the numerical results. By increasing the size and quantity of GFRP bars, the load-carrying capacity cannot be improved without simultaneously increasing the concrete maximum strength. The initial fracture load increased by 48.62% when the concrete maximum strength was increased from 25 to 45 MPa.

S. Kumer (2022) [10] carried out a test on three RC slab specimens with CFRP, three specimens with BFRP, and a reference slab with steel bars to compare the behavior of RC elements with steel, CFRP, and BFRP. It was shown that after loading, the BFRP-RC and CFRP-RC slabs both showed high deflection with wider cracking compared to the steel-RC slab. Although the axial stiffness of BFRP and CFRP bars is 16% and 41% lower than that of steel rebar, respectively, the stiffness of the steel-RC slab upon cracking was 48% and 64% for the BFRP-RC and CFRP-RC slabs, respectively. The steel-RC slab failed due to tension failure due to steel yielding, and the FRP-RC slabs failed due to punching shear.

To the authors' knowledge, several investigations have been conducted to compare the performance of RCBs reinforced with steel bars and those with FRP bars [7, 8, and 9]. However, the conclusions related to ductility for instance, derived from such research, may not be realistic since the ductility measures used for the comparison are based on those conventional definitions of the ductility of beams with steel reinforcement. Instead, the exhibited strain energy, as a reflection of structure performance, may be an alternative measure to be employed in the comparison.

The aim of this study is to assess the use of FRP bars as an alternative passive reinforcement in RCBs. A numerical investigation is conducted to assess the

performance of RCBs with FRP bars compared with conventional steel bars. This investigation takes into consideration material nonlinearity through the use of a three-dimensional nonlinear finite element analysis (NFEA) using the ABAQUS software. In the library of ABAQUS software [11], the user is given access to a variety of material models and element types that make it possible to precisely simulate the intricate nonlinear behavior of RC structures. As accurate nonlinearity simulation of such elements is essential, this study used the concrete damage plasticity model (CDPM) as recommended [12].

Methods

The ABAQUS software library contains a wide variety of material models and element types. This enables the better modeling of different structures.

Concrete modeling using CDPM

CDPM, which accurately simulates the complex behavior of concrete, has been utilized in several studies [12–15]. The two main failure modes in this plasticity-based model are crushing and cracking. A number of factors, such as those for plasticity, the uniaxial behavior of concrete, and the parameters of damage in both tension, d_t, and compression,d_c, must be defined to apply this model.

Concrete's uniaxial stress–strain relation

Figure 3a illustrates how Thorenfeldt et al. [16] developed a stress–strain model that is used to describe the concrete behavior under one-directional compression loading. This model is given by Eq. (1), where the strain ε_0 is related to the concrete maximum strength, $f_c\prime$, which is calculated using k and n model parameters [17]. In contrast, Jowkarmeimandi and Aslani [18] gave a model to describe the behavior of the concrete material under tension (Fig. 3b). The ascending branch in this model is a straight line that rises to the strain, ε_{to}, and the tensile strength of concrete, f_t. The strain degradation behavior in this model is according to Eq. (2), where ε_t is the strain at the post-cracking region corresponding to a stress σ_t.

$$\frac{f_c}{f_c'} = \frac{n\left(\frac{\varepsilon_c}{\varepsilon_0}\right)}{n-1+\left(\frac{\varepsilon_c}{\varepsilon_0}\right)^{nk}} \tag{1a}$$

$$\varepsilon_0 = \frac{f_c^{'}}{E_c}\frac{n}{n-1} \tag{1b}$$

$$n = 0.8 + \frac{f_c^{'}MPa}{17.25} \tag{1c}$$

$$k = 0.67 + \frac{f_c^{'}MPa}{62} \geq 1 \tag{1d}$$

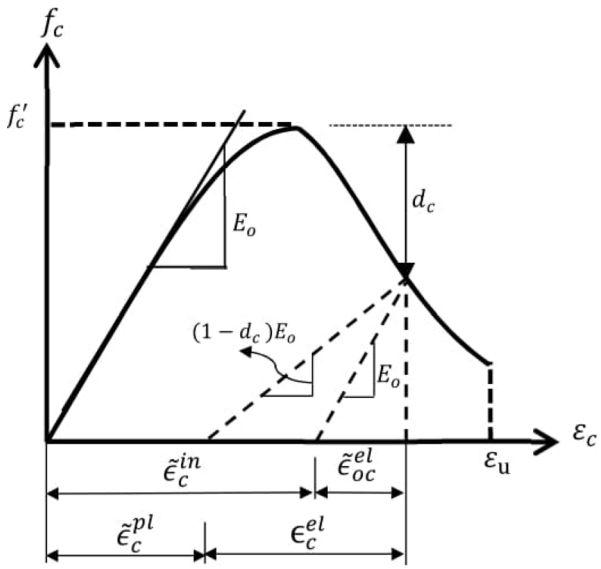

(a) Concrete's compression uniaxial behavior

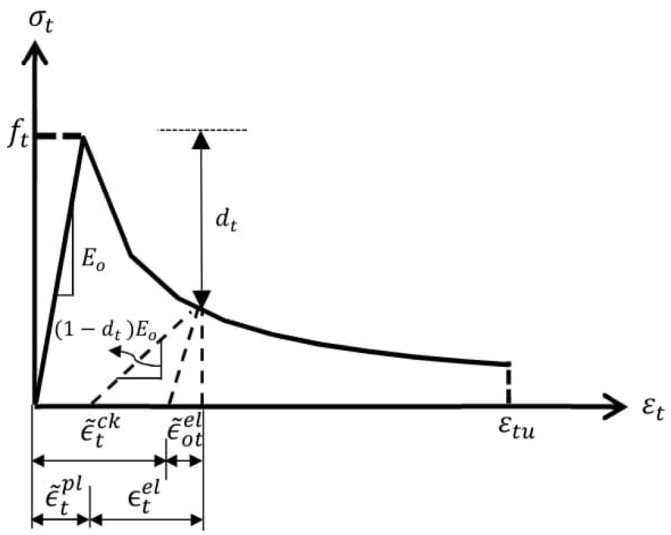

(b) Concrete's tension uniaxial behavior

Fig. 3 Concrete's uniaxial behavior under compression and tension [11]. **a** Concrete's compression uniaxial behavior. **b** Concrete's tension uniaxial behavior

$$\sigma_t = f_t \left(\frac{\varepsilon_{to}}{\varepsilon_t} \right)^{0.85} \tag{2}$$

The tensile strain that corresponds to the stress f_t is denoted by ε_{to}.

Major damage parameters

Figure 2 illustrates how both factors, which are provided by Eqs. (3) and (4) [19], are included in the strain degradation stage of the stress–strain relationship.

$$d_c = 1 - \frac{f_c}{f_c'} \tag{3}$$

$$d_t = 1 - \frac{\sigma_t}{f_t} \tag{4}$$

Concrete characteristics' definitions

An inelastic strain $\tilde{\epsilon}_c^{in}$ and the accompanying compressive stress f_c introduce the uniaxial stress–strain relationship in compression of concrete (Fig. 2a).

$$\tilde{\epsilon}_c^{in} = \epsilon_c - \tilde{\epsilon}_{oc}^{el}, \tilde{\epsilon}_{oc}^{el} = \frac{f_c}{E_o} \tag{5}$$

where E_o is the concrete's initial elastic modulus. Using the provided data of d_c, the inelastic strain $\tilde{\epsilon}_c^{in}$ is turned into plastic stain $\tilde{\epsilon}_c^{pl}$ as follows:

$$\tilde{\epsilon}_c^{pl} = \tilde{\epsilon}_c^{in} - \frac{d_c}{(1-d_c)}\frac{\sigma_c}{E_0} \tag{6}$$

Similar to this, the relationship of the stress and the induced strain is expressed in terms of a cracking strain $\tilde{\epsilon}_t^{ck}$ under uniaxial tension;

$$\tilde{\epsilon}_t^{ck} = \epsilon_t - \tilde{\epsilon}_{ot}^{el}, \tilde{\epsilon}_{ot}^{el} = \frac{f_t}{E_o} \tag{7}$$

Elastic modulus

In this study, the elastic modulus, E_o, of normal strength concrete, NSC, is calculated from the following ACI318-19 [20] formula.

$$E_o = 4700\sqrt{f_c'} \tag{8}$$

As for the high strength concrete, E_o is obtained according to the ACI Committee 363 [21].

$$E_o = 3300 + \sqrt{f_c'} + 6900(\text{MPa}) \tag{9}$$

For both normal and high strength concrete, it is assumed that Poisson's ratio is 0.20.

Plasticity parameters for the CDPM

Five parameters are needed to determine the yield (failure) surface of concrete [11, 22]. The following are the parameters that have been selected for the developed numerical model: 36 degrees is the dilation angle that is defined. 0.667 is chosen as the value for the parameter K_c. The viscosity parameter is measured at 0.00035 [23]. Eccentricity and σ_{b0}/σ_{c0} remain at their default values of 0.1 and 1.16, respectively [22].

Modeling of reinforcing bars

With a Poisson's ratio of 0.3 and a modulus of elasticity of $E_s = 200$ GPa, the reinforcing steel is defined as an elastic material at the first loading stage and after the yielding point, as a perfectly plastic material. As for the FRP bars, they are elastic material until failure [24], with an elastic modulus (E_f) changing according to their type. For modeling steel and FRP reinforcement in ABAQUS, these elements that are embedded into the concrete are often simulated as one-dimensional elements. The FRP failure is simulated as ductile damage, with the fracture strain equal to the strain at the failure stress, stress triaxiality, and strain rate equal to zero. But for the plastic properties, the plastic strain at the ultimate stress is equal to zero. An effective assessment of the interaction between concrete and reinforcement, including bond-slip, may be conducted indirectly using the CDPM in addition to tension stiffening of the concrete model components. This replicates how the load is transferred across cracks via the reinforcing bars. This method has been used in this study for both types of reinforcement, and it has proved to lead to an acceptable accuracy. For verification of steel and FRP bar modeling, two simple models consisting of steel and FRP bars with a 500-mm length are loaded in their longitudinal direction. The variation of stress versus strain in such material is shown in Fig. 4.

Chosen elements

A 3D hexahedral element with eight nodes, C3D8R (Fig. 5a), is used to simulate the loading plates and the concrete in order to do the 3D analysis. In this element, each node has the ability to move in three directions. The element with two nodes T3D2 (Fig. 5b) has been utilized to simulate the reinforcement, whether it be steel or FRP. In this element, each node has the same degrees of freedom as the ones in the concrete element.

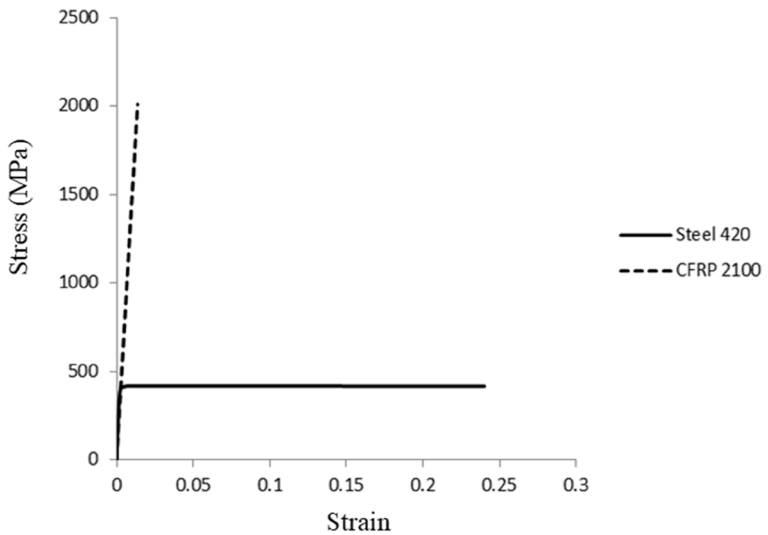

Fig. 4 Response of stress–strain in FRP and steel bars

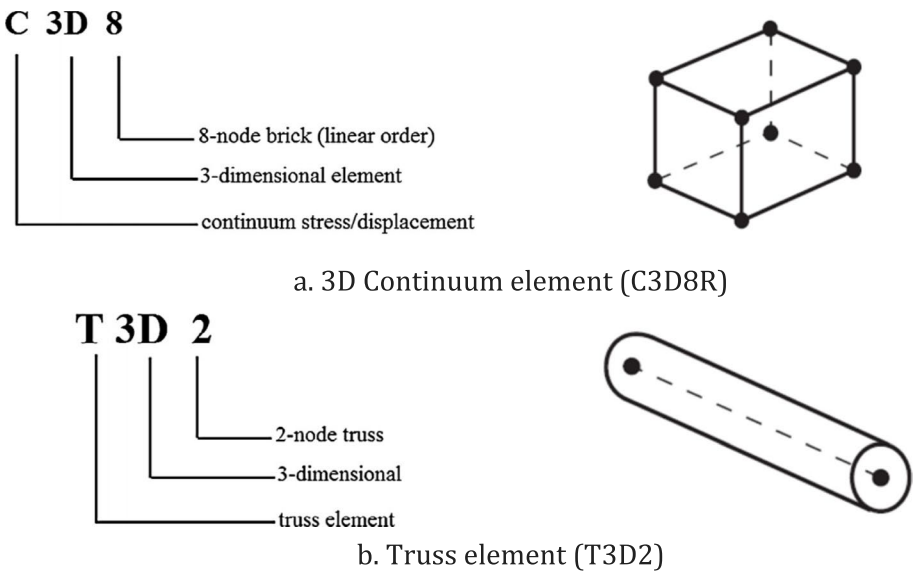

Fig. 5 Chosen element types for numerical modeling [13]. **a** 3D continuum element (C3D8R). **b** Truss element (T3D2)

Verification of the finite element modeling

Description of the verification specimens

To check the accuracy of the constructed numerical models, the experimental data obtained by Karayannis et al. [8] and Alam and Hussein [25] have been used. The two mentioned experiments used concrete beams reinforced with CFRP or GFRP in addition to steel bars. Figure 6 shows the configurations of the tested beams from the two studies.

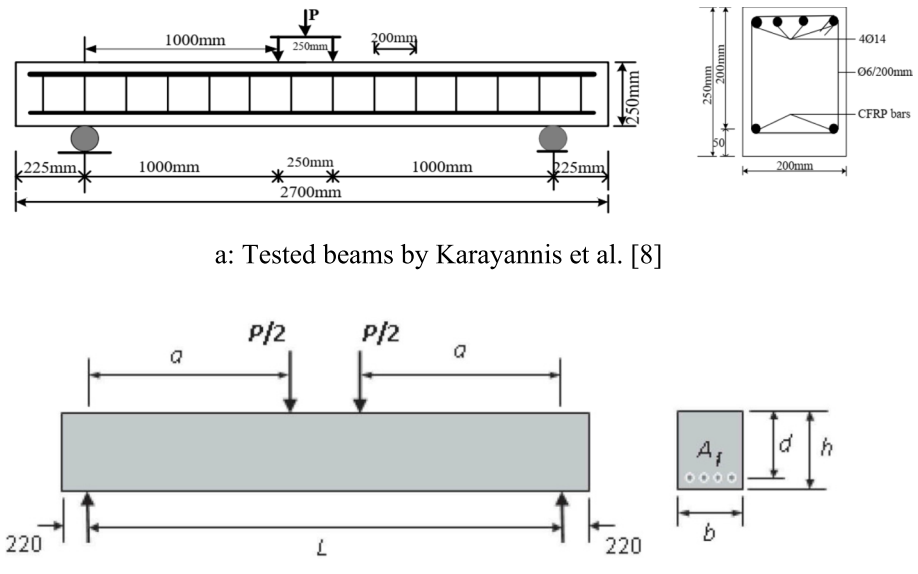

Fig. 6 Specimens description of experimental investigations 1 and 2. **a** Tested beams by Karayannis et al. [8]. **b** Tested beams by Alam and Hussein [25]

In the first experimental investigation [8], the concrete's compressive and tensile strengths were $f_c' = 29.10$MPa and $f_t = 2.42$MPa, respectively. The deformed steel bars' yield strength, f_y, was 555 MPa for 10-mm-diameter bars, 545 MPa for 12-mm-diameter bars, and 550 MPa for 14-mm-diameter bars. The stirrups used have a diameter of 6 mm and a yield strength of 310 MPa. The CFRP bars used in this investigation were M9, M10, and M11 with tensile strength $f_{fu} = 1800$MPa and elasticity modulus $E_f = 130$GPa.

In the second experimental investigation [25], only reinforcement from GFRP bars were used. The bars of diameter 12 mm had tensile strength ($f_{fu} = 786$MPa), elasticity modulus ($E_f = 46.3$GPa), and cross-sectional area of 127mm^2. As for the bars of diameter 16 mm, the tensile strength ($f_{fu} = 751$MPa), elasticity modulus ($E_f = 48.2$GPa), and cross-sectional area of 198mm^2.

The specimens of the first experimental investigation [8] are simply supported beams of 2700 mm length, 200 mm width, and 250 mm total depth. The longitudinal reinforcement of M1 and M2 is steel bars and that of M9, M10, and M11 is CFRP bars, whereas all the specimens had steel stirrups, as shown in Table 1.

The specimens of the second experimental investigation [25] are simply supported beams with different span lengths and section dimensions, whereas the longitudinal reinforcement of all the specimens was GFRP as tabulated in Table 2.

Meshing and loading boundary conditions

The geometry of the FEM of the tested specimens and reinforcement configuration are shown in Fig. 7a. The imposed support boundary constraints are (the displacement $U_y = 0$). To take advantage of symmetry, only halves of the specimens were analyzed

Table 1 Specimen description of the first experimental investigation [8]

Group	Model	b (mm)	h (mm)	L (mm)	Top RFT	Bottom RFT	Type of bottom RFT	Stirrups	f_c'(MPa)
1	M1	200	250	2700	4Φ14	2Φ10	Steel	Φ6@200	29.1
	M2					2Φ12			
2	M9	200	250	2700	4Φ14	2Φ10	CFRP	Φ6@200	29.1
	M10					2Φ12			
	M11					3Φ12			

Table 2 Specimen description of the second experimental investigation [25]

Group	Model	b (mm)	h (mm)	L (mm)	Bottom RFT	Type	f_c'(MPa)
1	G-1.5	250	350	1700	2Φ12 + 2Φ16	GFRP	35
	G-2.5	250	350	2400	2Φ12 + 2Φ16	GFRP	40
	G-3.5	250	350	3100	2Φ12 + 2Φ16	GFRP	40
2	G-500	250	500	3100	3Φ12 + 3Φ16	GFRP	45
	G-500–70	250	500	3100	7Φ16	GFRP	75
	G-650	300	650	3600	8Φ16	GFRP	37
	G-650–70	300	650	3600	12Φ16	GFRP	75

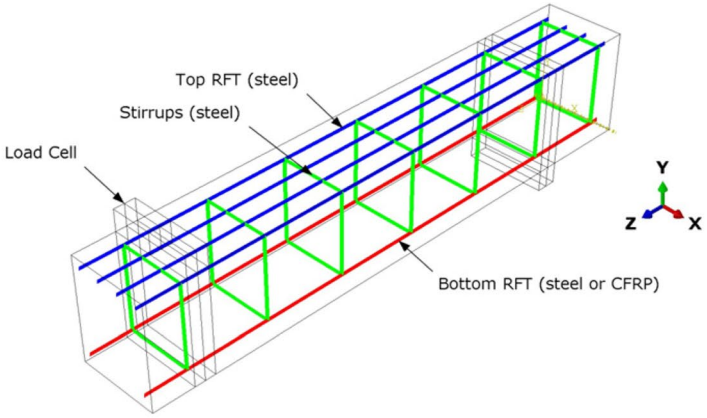

a: Steel and CFRP reinforcement configuration

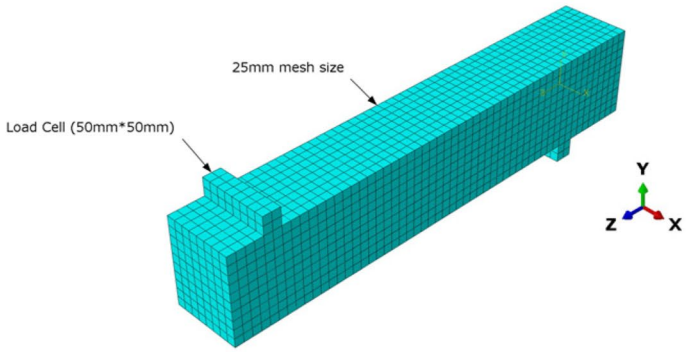

b: Specimen meshing

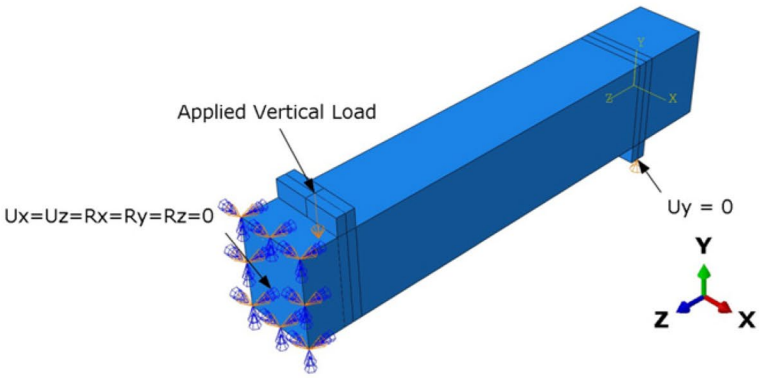

c: Specimen boundary conditions

Fig. 7 Specimen description. **a** Steel and CFRP reinforcement configuration. **b** Specimen meshing. **c** Specimen boundary conditions

with the boundary conditions applied at mid-span (the rotation $R_x = R_y = R_z = 0$ and the displacement $U_x = U_z = 0$) (Fig. 7c). The contact surface between the RCB and loading plate is introduced utilizing a tie constraint. To better represent the experiment conditions, a small uniform mesh size (25 mm) for all elements was used

(Fig. 7b). Four loading plates are used with cross-section50 mm × 50 mm and 200 mm in length with 25-mm mesh size.

Results and discussion

The behavior of RCBs (load–deflection curves (P/2 versus δ)) obtained from the FEM, along with those from the tests, are plotted in Fig. 8. In addition, the peak strength with the maximum corresponding deflection, from the finite element and the tests, is given in Tables 3 and 4. The comparison given in the figure and the tables show how accurate the FE model is in simulating the behavior of the RC beams reinforced with either steel bars or FRP (carbon or glass) bars.

The second step to verify the FE result is to compare the crack pattern of tested beams as shown in Fig. 9a with FE model crack pattern as shown in Fig. 9b.

Parametric study

To assess the role of FRP as a passive reinforcement of beams, a parametric study is performed by considering different reinforcement ratios. In this study, certain characteristics of beam behavior are examined: ductility, stiffness, and strain energy. In all the examined specimens, tension failure was guaranteed by increasing the ratio of compression reinforcement. The behavior of the RCBs with FRP is compared with their counterparts reinforced with steel.

Modes of failure of RCBs with FRP bars

Two mechanisms control the RCBs with FRP bars' ultimate flexural strength: FRP rupture (Fig. 10a) or concrete crushing (Fig. 10b) [5]. Balanced failure takes place when FRP rupture and concrete crushing occur simultaneously (Fig. 10c). The balanced reinforcement ratio, defined by Eq. (10) corresponding to this case, can be obtained from Eq. (11).

$$\rho_f = \frac{A_f}{bd} \tag{10}$$

$$\rho_{fb} = 0.85\beta_1 \frac{f_c'}{f_{fu}} \frac{E_f \varepsilon_{cu}}{E_f \varepsilon_{cu} + f_{fu}} \tag{11}$$

Nominal flexural strength

Concrete crushing is the governing state when the FRP reinforcement ratio exceeds the balanced FRP reinforcement ratio, and the ACI Code can be used to approximate the stress distribution in the compression area as a rectangular block of stress. The stress of FRP bar (f_f) can be estimated from Eq. (12). If the value of f_f is greater than f_{fu}, the controlling state is FRP rapture, and the nominal strength can be calculated

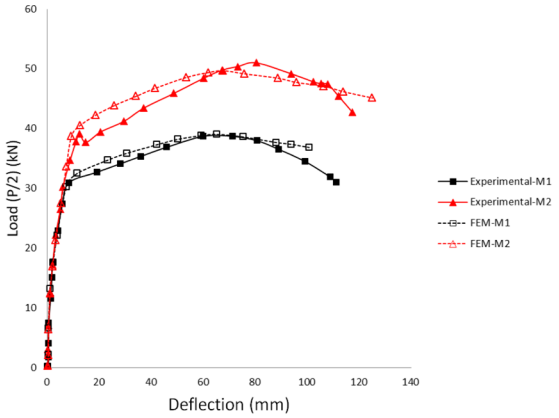

a: Results of specimens M1 and M2 of the first experimental investigation

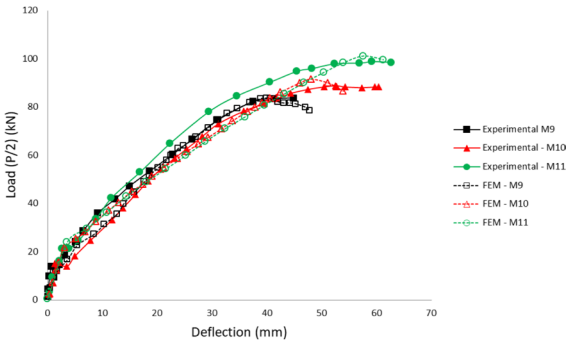

b: Results of specimens M9, M10 and M11 of the first experimental investigation

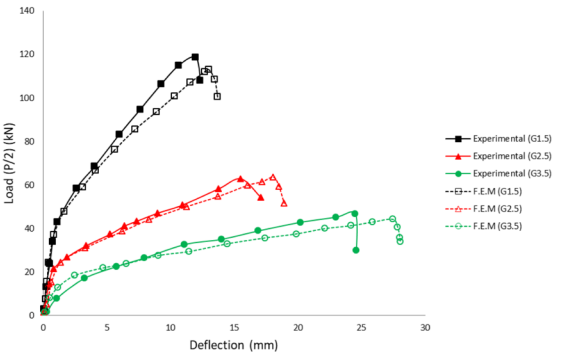

c: Results of the first group's specimens of the second experimental investigation

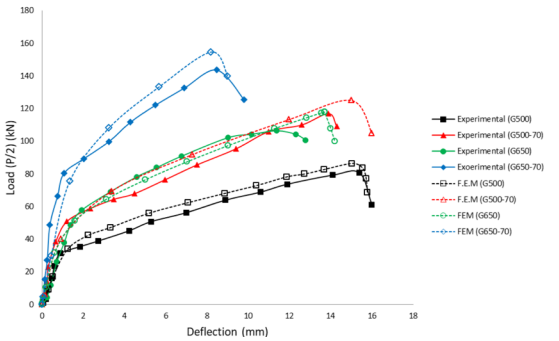

d: Results of the second group's specimens of the second experimental investigation

Fig. 8 Tested beams load–deflection curves. **a** Results of specimens M1 and M2 of the first experimental investigation. **b** Results of specimens M9, M10, and M11 of the first experimental investigation. **c** Results of the first group's specimens of the second experimental investigation. **d** Results of the second group's specimens of the second experimental investigation

Table 3 Comparing the results of the first experimental investigation

Group	Model	V_{Exp} (kN)	V_{FEM} (kN)	δ_{Exp} (mm)	δ_{FEM} (mm)	V_{Exp}/V_{FEM}	$\delta_{Exp}/\delta_{FEM}$
1	M1	39.2	39	110	100	1.005	1.1
	M2	51	50	117	125	1.02	0.936
2	M9	84	83	45	48	1.012	0.937
	M10	88	92	60	54	0.957	1.11
	M11	99	101	63	62	0.98	1.02

Table 4 Comparing the results of the second experimental investigation

Group	Model	V_{Exp} (kN)	V_{FEM} (kN)	δ_{Exp} (mm)	δ_{FEM} (mm)	V_{Exp}/V_{FEM}	$\delta_{Exp.}/\delta_{FEM}$
1	G-1.5	108	113	12	13	0.95	0.923
	G-2.5	63	63.3	17	18	0.99	0.94
	G-3.5	47	45	25	27	1.04	0.926
2	G-500	81	86	16	15	0.94	1.06
	G-500–70	117	125	14	16	0.936	0.875
	G-650	106	118	13	14	0.9	0.928
	G-650–70	143	155	10	9	0.923	1.11

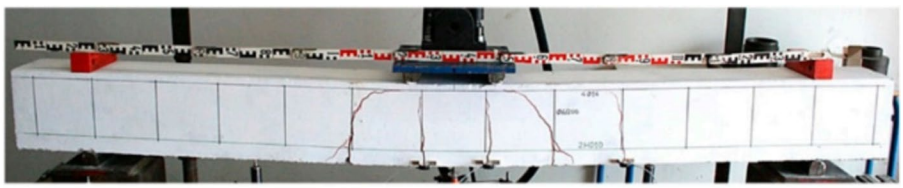

a: Crack pattern of tested beam M1

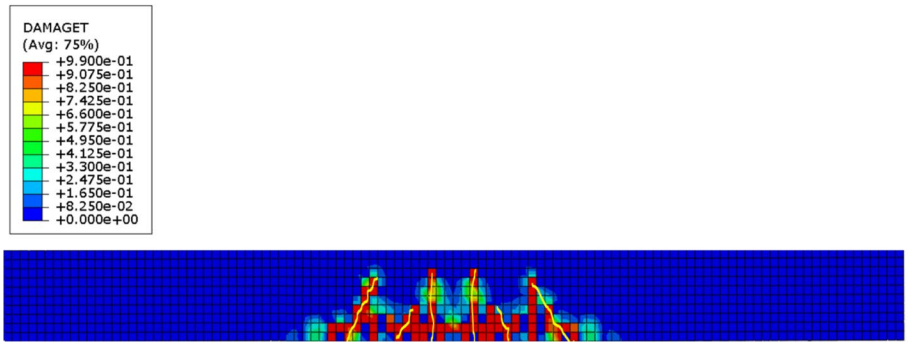

b: Crack pattern in model of beam M1

Fig. 9 Verifying the crack pattern of tested beams with FE model. **a** Crack pattern of tested beam M1. **b** Crack pattern in model of beam M1

from Eq. (13), else the controlling state is concrete crushing, and the nominal strength can be calculated from Eq. (14).

$$f_f = \left(\sqrt{\frac{(E_f\varepsilon_{cu})^2}{4}\frac{0.85\beta_1 f_c'}{\rho_f}E_f\varepsilon_{cu}} - 0.5E_f\varepsilon_{cu}\right) \le f_{fu} \tag{12}$$

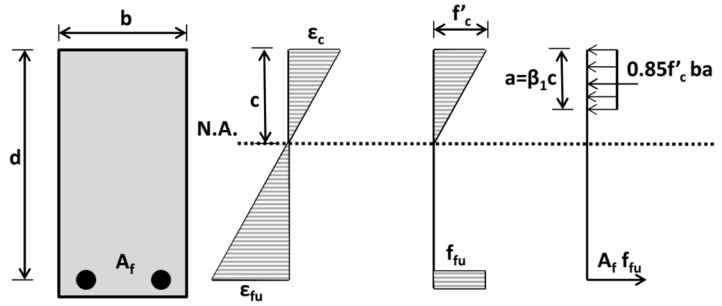

a: FRP rapture (concrete strain may be nonlinear)

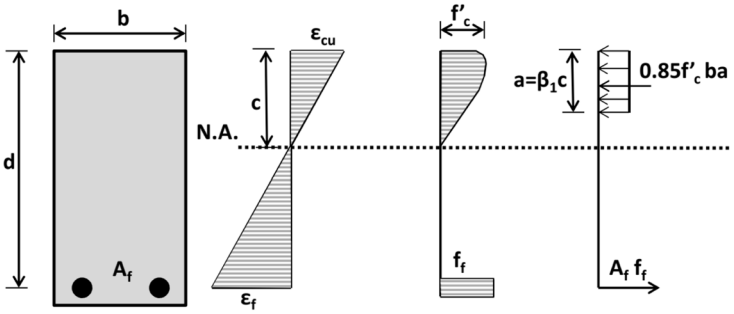

b: Concrete crushing

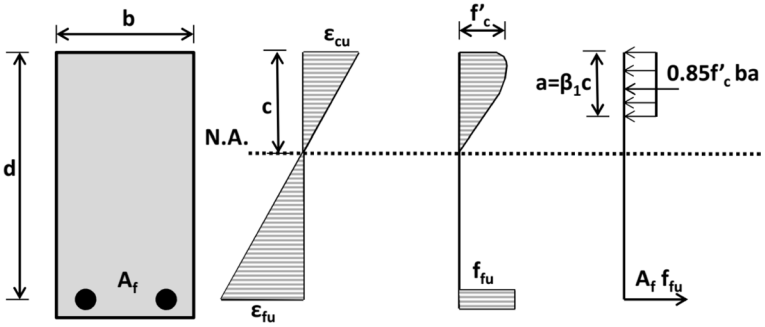

c: balanced failure

Fig. 10 Modes of failure of RCBs with FRP bars [5]. **a** FRP rapture (concrete strain may be nonlinear). **b** Concrete crushing. **c** balanced failure

For the case of FRP rupture failure

$$M_n = \rho_f f_u (1 - 0.59 \frac{\rho_f f_u}{f'_c}) bd^2 \tag{13}$$

For the case of concrete crushing failure

$$M_n = \rho_f f_f (1 - 0.59 \frac{\rho_f f_f}{f'_c}) bd^2 \tag{14}$$

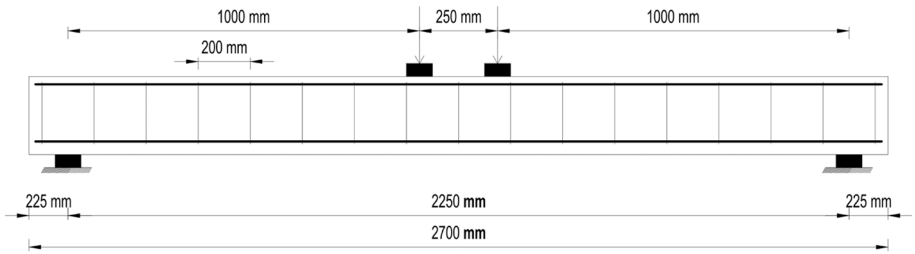

Fig. 11 Dimensions of investigated beams

Description of the investigated specimens

The study covers 38 shallow beams subjected to two concentrated loads. All examined beams are 2700 mm in length and 200 mm in width, as shown in Fig. 11, with variable depth (250 mm, 400 mm, and 600 mm), bottom reinforcement ratio (steel and CFRP bars), stirrups diameter and distribution, and concrete compressive strength (35 MPa, 40 MPa, 50 MPa, and 70 MPa). Four groups of beams were simulated (Table 5). Group 1 consists of 18 simply supported beams with a 250-mm depth; group 2 consists of eight simply supported beams with a 400-mm depth; group 3 consists of eight simply supported beams with a 600-mm depth, and group 4 consists of four of simply supported beams with a 400-mm depth with variable diameter and distribution of stirrups. The material properties of steel bars, FRP bars, and stirrups of all beams are given in Table 6. Four Load plates are used with cross-section 50 mm × 50 mm and 200 mm in length with 25 mm mesh size.

Results of parametric study

The results from the parametric study are discussed here in order to examine the role of the FRP as a passive reinforcement in comparison with the traditional steel bars.

Load–deflection relationship

The load–deflection (P/2 versus δ) curves of the modeled RCBs with CFRP bars and steel are shown in Fig. 12. Additionally, a comparison is made between the numerically calculated peak load of each analyzed beam and the estimates derived from the ACI440.1-R15 [5] equations, as presented in Table 7.

The load–deflection curve has been divided into two sections. The first segment describes the region of the beam that is not cracked and has a high flexure stiffness, almost like RCBs with steel bars. The load-deformation response and the cracking stiffness of the beams are reflected in the second part. After the initial crack, the beam becomes less stiff, and as the load increases, the CFRP bar ruptures and the steel bar starts to yield, leading to failure.

From the results for the modeled beams as presented in Fig. 12, it becomes clear that increasing the beam depth, the concrete strength, the size, and the number of steel or CFRP bars would all significantly increase the beam's carrying capacity. Upon comparing the load–deflection curves of RCBs with steel bars and those with CFRP bars, it is found

Table 5 Reinforcement details of the investigated beams

Model no		Section	Code	Top RFT	Bottom RFT	Type of bottom RFT	Stirrups	f_c'(MPa)
1	Group 1	200 mm × 250 mm	A-S1	4T14	2T10	Steel	5T6/m	35 MPa
2			A-S2		2T12			
3			A-S3		2T16			
4			A-F1		2T6	CFRP		
5			A-F2		2T8			
6			A-F3		2T10			
7			A-S4		2T10	Steel		40 MPa
8			A-S5		2T12			
9			A-S6		2T16			
10			A-F4		2T6	CFRP		
11			A-F5		2T8			
12			A-F6		2T10			
13			A-S7		2T10	Steel		50 MPa
14			A-S8		2T12			
15			A-S9		2T16			
16			A-F7		2T6	CFRP		
17			A-F8		2T8			
18			A-F9		2T10			
19	Group 2	200 mm × 400 mm	B-S1		2T16	Steel	5T8/m	50 MPa
20			B-S2		4T16			
21			B-F1		2T10	CFRP		
22			B-F2		4T10			
23			B-S3		2T16	Steel		70 MPa
24			B-S4		4T16			
25			B-F3		2T10	CFRP		
26			B-F4		4T10			
27	Group 3	200 mm × 600 mm	C-S1		2T16	Steel		50 MPa
28			C-S2		4T16			
29			C-F1		2T10	CFRP		
30			C-F2		4T10			
31			C-S3		2T16	Steel		70 MPa
32			C-S4		4T16			
33			C-F3		2T10	CFRP		
34			C-F4		4T10			
35	Group 4	200 mm × 400 mm	D-S1	4T14	2T16	Steel	5T6/m	50 MPa
36			D-S2		2T16		10T10/m	
37			D-F1		2T10	CFRP	5T6/m	
38			D-F2		2T10		10T10/m	

that RCBs with CFRP bars have a higher ultimate failure load but a much smaller yield plateau compared to the RCBs with traditional steel bars.

The load–deflection behavior of the two models (B-F2 and C-F2) exhibits different behavior because of the yielding of the compression reinforcement before concrete crushing or CFRP rapture, as shown in Fig. 13. This behavior shows that RCBs with

Table 6 Material properties of the investigated models

Steel bars	Yield stress	500 MPa
	Tensile strength	690 MPa
	Modulus of elasticity	200 GPa
	Poisson's ratio	0.3
GFRP	tensile strength	2100 MPa
	Modulus of elasticity	150 GPa
Steel Stirrups	Yield stress	300 MPa
	Tensile strength	420 MPa
	Modulus of elasticity	200 GPa
	Poisson's ratio	0.3

CFRP bars can reflect a higher ductility, but only in the presence of an optimum ratio of compression reinforcement.

Crack pattern

Crack pattern is one of the tools to compare the behavior of different RC elements. In the current study, the crack pattern, concrete, and bars stresses of RCBs with steel and FRP bars for two models (A-S1 and A-F1) are compared, as shown in Fig. 14. Crack pattern for the model with CFRP bars (A-F1) is more propagated because of CFRP's low modulus of elasticity, which cause a relatively large strain at the same load case.

Strain energy

The strain energy represents the area under the load–deflection curve and provides information about the ductility [26]. To compare RCBs with steel bars and those with CFRP bars, Table 8 shows the results for all tested beams together with the computed strain energy of each beam. With the exception of unrealistically high compression reinforcement, the strain energy of RCBs with CFRP bars is often substantially lower than that of RCBs with conventional steel bars, according to Table 8.

Conclusions

The NFEA has been utilized to examine how RCBs with FRP bars behave under the action of monotonic vertical loading regimes. It has been demonstrated that the solution scheme yields results with very high accuracy when compared with experimental tests. A parametric study has been performed in order to assess the role of FRP as a passive reinforcement of concrete beams in comparison with conventional steel bars. Also, the strength predictions of the RCBs with FRP bars from the numerical

(See figure on next page.)

Fig. 12 The tested beams' load–deflection curves. **a** The first six models (200 mm × 250 mm) in the first group's load–deflection curves. **b** The second six models (200 mm × 250 mm) in the first group's load–deflection curves. **c** The third six models (200 mm × 250 mm) in the first group's load–deflection curves. **d** The second group's load–deflection curves (200 mm × 400 mm). **e** The third group's load–deflection curves (200 mm × 600 mm). **f** The fourth group's load–deflection curves (200 mm × 400 mm)

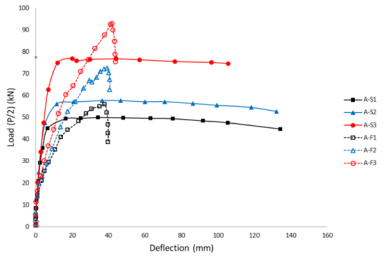

a: The first six models (200mmx250mm) in the first group's load-deflection curves

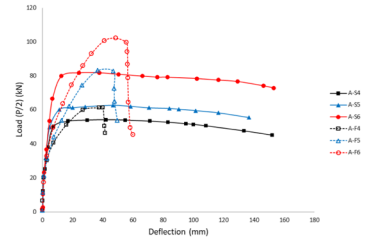

b: The second six models (200mmx250mm) in the first group's load-deflection curves

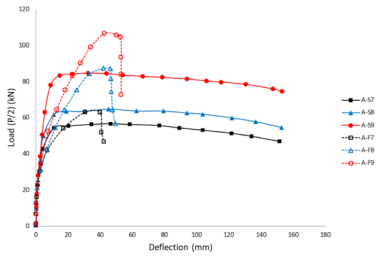

c: The third six models (200mmx250mm) in the first group's load-deflection curves

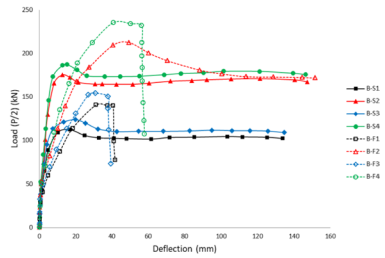

d: The second group's load-deflection curves (200mmx400mm)

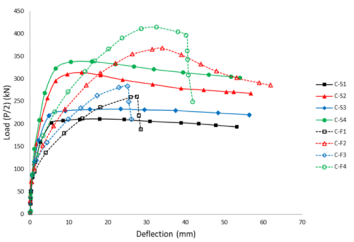

e: The third group's load-deflection curves (200mmx600mm)

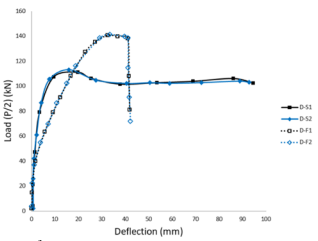

f: The fourth group's load-deflection curves (200mmx400mm)

Fig. 12 (See legend on previous page.)

Table 7 Comparison between F.E.M results and ACI Code results

No	Beam code	FEM results V_{FEM} (kN)	ACI code V_{ACI} (kN)	Ratio V_{FEM}/V_{ACI}
1	A-S1	50	38	1.31
2	A-S2	57	54	1.05
3	A-S3	77	93	0.82
4	A-F1	55	50	1.1
5	A-F2	72	79	0.91
6	A-F3	93	95	0.98
7	A-S4	54	39	1.38
8	A-S5	62	55	1.12
9	A-S6	82	94	0.87
10	A-F4	61	50	1.22
11	A-F5	65	84	0.78
12	A-F6	102	101	1.01
13	A-S7	57	40	1.42
14	A-S8	64	56	1.14
15	A-S9	85	95	0.89
16	A-F7	63	51	1.23
17	A-F8	87	86	1.01
18	A-F9	106	110	0.96
19	B-S1	112	151	0.74
20	B-S2	175	297	0.59
21	B-F1	140	112	1.25
22	B-F2	187	159	1.17
23	B-S3	140	156	0.89
24	B-S4	212	302	0.70
25	B-F3	154	127	1.21
26	B-F4	232	204	1.13
27	C-S1	211	236	0.89
28	C-S2	314	460	0.68
29	C-F1	232	191	1.21
30	C-F2	338	360	0.94
31	C-S3	260	237	1.09
32	C-S4	367	468	0.78
33	C-F3	283	193	1.46
34	C-F4	414	377	1.09
35	D-S1	112	151	0.74
36	D-S2	112	151	0.74
37	D-F1	140	112	1.25
38	D-F2	140	112	1.25

solutions have been compared with those from the ACI 440-1R [3], and the comparison was very satisfactory. The findings of this study can be summarized in the following:

1. RCBs with CFRP bars can sustain a higher ultimate failure load but with much less ductility in terms of deformability (or yield plateau) when compared to RCBs with traditional steel bars.

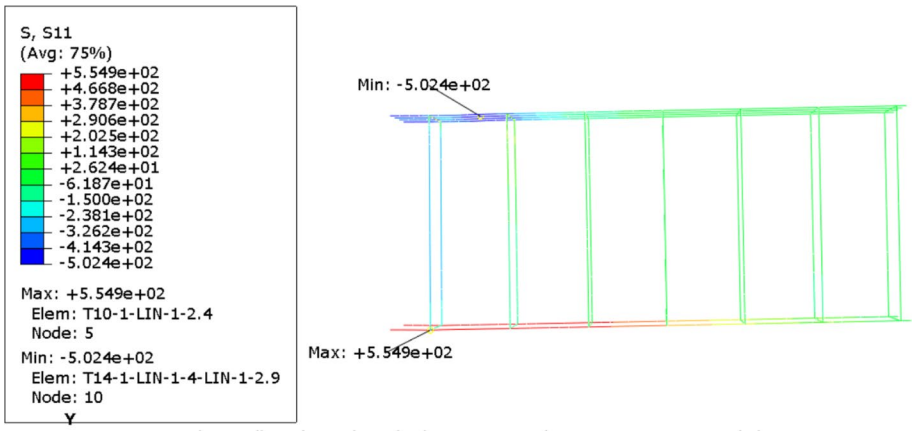

a: Top Steel and bottom CFRP stresses of the model B-F2

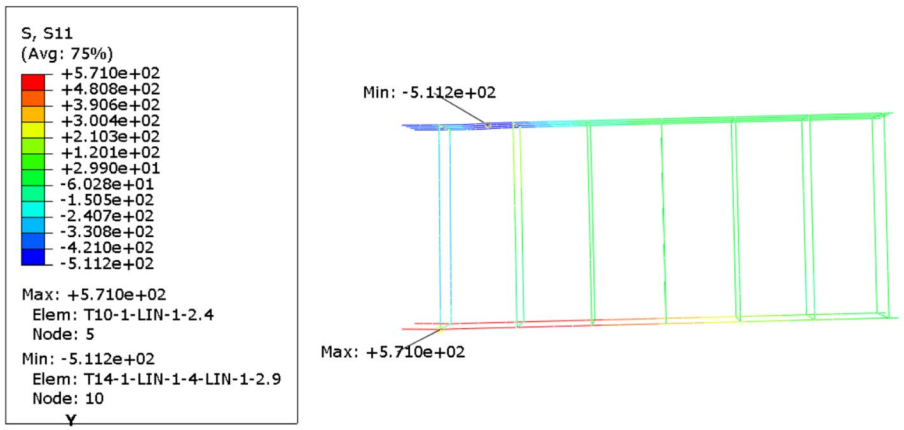

b: Top steel and bottom CFRP stresses of the model C-F2

Fig. 13 Top steel and bottom CFRP stresses of the two models (B-F2–C-F2). **a** Top steel and bottom CFRP stresses of the model—B-F2. **b** Top steel and bottom CFRP stresses of the model—C-F2

2. The strain energy of RCBs with CRFP is about 25–50% of that of RCBs with traditional steel bars. This indicates that RCBs with CFRP are much less ductile than RCBs with conventional steel bars.
3. RCBs with small reinforcement ratios of steel or CFRP are almost similar in terms of the resulting strain energy.

(See figure on next page.)

Fig. 14 Crack pattern, concrete stress, bars stresses, and deflection for the two models A-S1 and A-F1. **a** First crack propagation for model A-S1. **b** First crack propagation for model A-F1. **c** Concrete stresses at first crack for model A-S1. **d** Concrete stresses at first crack for model A-F1. **e** Steel bars stresses at first crack for model A-S1. **f** FRP bars stresses at first crack for model A-F1. **g** Crack pattern propagation at 20 kN downward for model A-S1. **h** Crack pattern propagation at 20 kN downward for model A-F1. **i** Plastic strain (PE33) for model A-S1. **j** Plastic strain (PE33) for model A-F1. **k** Maximum principal plastic strain for model A-S1. **l** Maximum principal plastic strain for model A-F1

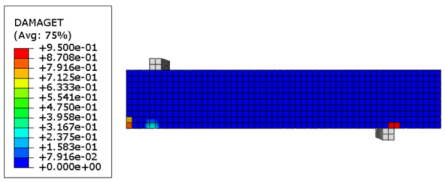

a: First crack propagation for model A-S1

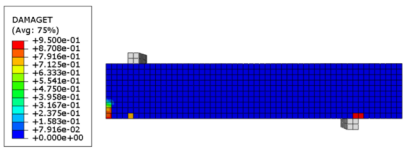

b: First crack propagation for model A-F1

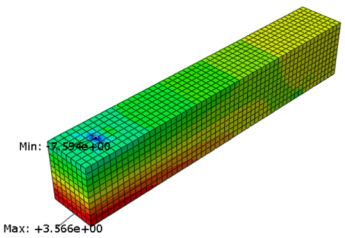

c: Concrete stresses at first crack for model A-S1

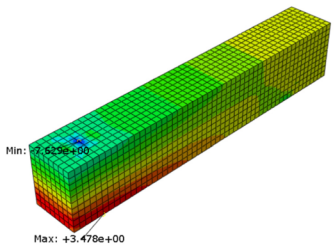

d: Concrete stresses at first crack for model A-F1

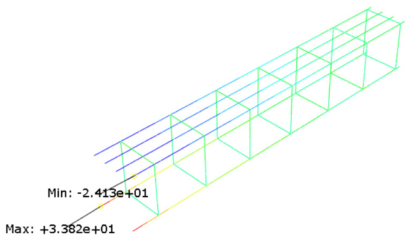

e: Steel bars stresses at first crack for model A-S1

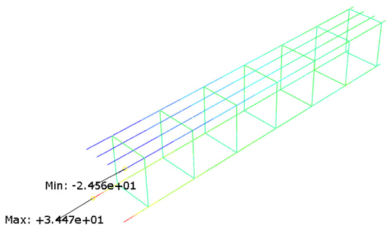

f: FRP bars stresses at first crack for model A-F1

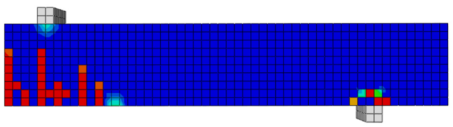

g: Crack pattern propagation at 20 kN downward for model A-S1

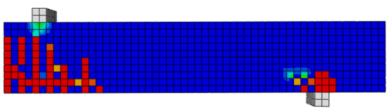

h: Crack pattern propagation at 20 kN downward for model A-F1

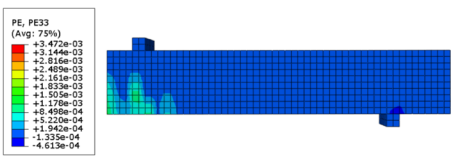

i: Plastic strain (PE33) for model A-S1

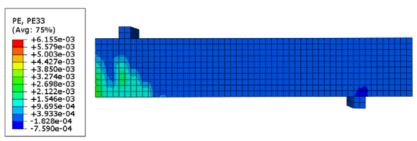

j: Plastic strain (PE33) for model A-F1

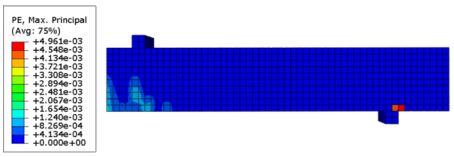

k: Maximum principal plastic strain for model A-S1

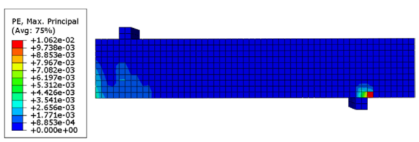

l: Maximum principal plastic strain for model A-F1

Fig. 14 (See legend on previous page.)

Table 8 Strain energy of tested beams

RCBs with steel bars		RCBs with CFRP bars		Strain energy $_{CFRP}$/strain energy $_{Steel}$
Beam code	**Total strain energy (kN.m)**	**Beam code**	**Total strain energy (kN.m)**	
A-S1	6.378	A-F1	1.487	23.3%
A-S2	7.277	A-F2	2.094	28.7%
A-S3	7.733	A-F3	2.755	35.6%
A-S4	7.697	A-F4	2.104	27.3%
A-S5	8.062	A-F5	3.192	39.5%
A-S6	11.768	A-F6	4.671	39.7%
A-S7	7.998	A-F7	2.201	27.5%
A-S8	9.270	A-F8	3.294	35.5%
A-S9	12.167	A-F9	4.714	38.7%
B-S1	13.694	B-F1	4.444	32.4%
B-S2	24.335	B-F2	26.553	109.1%
B-S3	14.935	B-F3	4.596	30.1%
B-S4	25.495	B-F1	10.676	41.8%
C-S1	10.577	C-F1	5.665	53.5%
C-S2	15.852	C-F2	18.449	116.3%
C-S3	12.491	C-F3	5.674	54.4%
C-S4	16.733	C-F4	13.732	82.1
D-S1	13.694	D-F1	4.444	32.4%
D-S2	13.694	D-F1	4.444	32.4%

4. RCBs with CFRP can similarly behave as beams with conventional steel bars in terms of ductility if the compression reinforcement is used with an optimum ratio to enable the yielding of compression reinforcement before concrete crushing or CFRP failure.
5. A set of precautions must be considered when using CFRP in RCBs as a passive reinforcement due to its limited level of ductility.

Abbreviations

FRP Fiber reinforced polymer
RC Reinforced concrete
GFRP Glass fiber-reinforced polymer
CFRP Carbon fiber-reinforced polymer
RCB Reinforced concrete beam

Acknowledgements
Not applicable

Authors' contributions
All three authors collaborated in the research. M.A. was responsible for the research itself including the literature review and numerical modeling work. Authors S.E. and B.A. were responsible for revising, guiding, and advising throughout the research process. All authors read and approved the final manuscript.

Funding
Not applicable.

Availability of data and materials
All data and material can be obtained from the corresponding author upon request.

Declarations

Competing interests
The authors declare that they have no competing interests.

Received: 1 December 2023 Accepted: 1 April 2024
Published online: 10 April 2024

References

1. Sammen SS, Ahmed QW, I-Karawi SN (2019) Nonlinear Finite Element Analysis of Concrete Beam Reinforced with Fiber Reinforced Polymer (FRM). In IOP Conference Series: Materials Science and Engineering, vol 518. IOP Publishing, p 022086
2. Suryanto B, Morgan R, Han AL (2016) Predicting the response of shear-critical reinforced concrete beams using response-2000 and SNI 2847: 2013. Civil Eng Dimension 18(1):16–24
3. Einde L, Zhao L, Seible F (2003) Use of FRP composites in civil structural applications. Constr Build Mater 17:389–403
4. ACI Committee (2001) Guide for the design and construction of concrete reinforced with FRP bars. American Concrete Institute
5. Afifi M, Mohamed H, Benmokrane B. (2013) axial capacity of circular concrete columns reinforced with GFRP bars and spirals. Am Soc Civil Eng. https://doi.org/10.1061/(ASCE)CC.1943-5614.0000438
6. Abed F, El-Mesalami N., El-Refai A. Compressive behaviour of glass fiber-reinforced polymer (GFRP) reinforced concrete columns. 10th International Conference on FRP Composites in Civil Engineering (pp.851–858). https://doi.org/10.1007/978-3-030-88166-5_73
7. Adam M, Said M, Mahmoud AA, Shanour AS (2015) Analytical and experimental flexural behavior of concrete beams reinforced with glass fiber reinforced polymers bars. Constr Build Mater 84:354–366
8. Karayannis CG, Kosmidou PM, Chalioris CE (2018) Reinforced concrete beams with carbon-fiberreinforcedpolymer bars—Experimental study. Fibers 6(4):99
9. Salih R, Fangyuan Z (2019) Numerical investigation of the behavior of reinforced concrete beam reinforced with FRP bars. Civil Eng J 5(11):2296–2308
10. Shill S, Garcez E, Al-Ameri R, Subhani M. (2022) Performance of two-way concrete slabs reinforced with basalt and carbon FRP rebars. J Composite Sci. https://doi.org/10.3390/jcs6030074
11. Simulia (2014) Abaqus analysis user's guide. Dassault Systèmes Simulia Corp, Providence
12. Genikomsou AS, Polak MA (2015) Finite element analysis of punching shear of concrete slabs using damaged plasticity model in ABAQUS. Eng Struct 98:38–48
13. El-Naqeeb MH, Abdelwahed BS, El-Metwally SE (2022) Numerical investigation of RC exterior beam-column connection with different joint reinforcement detailing. Structures 38:1570–1581
14. Dabiri H, Kaviani A, Kheyroddin A (2020) Influence of reinforcement on the performance of non-seismically detailed RC beam-column joints. J Building Eng 31:101333
15. El-Naqeeb MH, Abdelwahid BS, El-Metwally SE (2022) Strength of exterior beam-column connections considering column axial stress: numerical investigation. Jordan J of Civil Eng 16(2):262–283
16. Thorenfeldt E, Tomaszewicz A, Jensen JJ (1987) Mechanical properties of high strength concrete and application to design. Proceedings of the Symposium: Utilization of High-Strength Concrete, Stavanger, pp 149–159
17. Wight JK, MacGregor JG (2012) Reinforced concrete: mechanics and design. Pearson Education Inc, Upper Saddle River, New Jersey
18. Aslani F, Jowkarmeimandi R (2012) Stress–strain model for concrete under cyclic loading. Mag Concr Res 64(8):673–685
19. Jankowiak T, Lodygowski T (2005) Identification of parameters of concrete damage plasticity constitutive model. Foundations Civil Environ Eng 6(1):53–69
20. ACI 318 (2019) Building code requirements for structural concrete. American Concrete Institute (ACI), Farmington Hills
21. ACI 363 (1997) Report on High-Strength Concrete, ACI Manual of Concrete Practice. American Concrete Institute (ACI), Farmington Hills, p 55
22. Sümer Y, Aktaş M (2015) Defining parameters for concrete damage plasticity model. Challenge J of Struct Mech 1(3):149–155
23. Demir A, Ozturk H, Edip K, Stojmanovska M, Bogdanovic A (2018) Effect of viscosity parameter on the numerical simulation of reinforced concrete deep beam behaviour. J Sci Technol 8(3):50–56
24. Teng JG, Chen JF, Smith ST, Lam L (2002) FRP: strengthened RC structures. p 266
25. Alam M, Hussein A (2019) Finite element modelling of shear critical glass fibre-reinforced polymer (GFRP) reinforced concrete beams. International J Of Modelling and Simulation, Taylor & Francis
26. Hearn EJ (1997) Mechanics of Materials 1, 3rd edn. Butterworth Heinemann, Oxford

Publisher's Note